# Uncertainties in estimating winter balance from direct measurements of snow depth and density on alpine glaciers

Alexandra PULWICKI,[1] Gwenn E. FLOWERS,[1] Valentina RADIĆ,[2]

[1] *Department of Earth Sciences, Faculty of Science, Simon Fraser University, Burnaby, BC, Canada*
[2] *Department of Earth, Ocean and Atmospheric Sciences, Faculty of Science, University of British Columbia, Vancouver, BC, Canada*
*Correspondence: Alexandra Pulwicki <apulwick@sfu.ca>*

**ABSTRACT. Accurately estimating winter surface mass balance (WB) on glaciers is central to assessing glacier health and predicting glacier runoff. However, measuring and modelling snow distribution is inherently difficult in mountainous terrain, resulting in high uncertainties in estimates of WB. Our work focuses on uncertainty attribution within the process of converting direct measurements of snow depth and density to estimates of WB. We collected more than 9000 direct measurements of snow depth across three glaciers in the St. Elias Mountains, Yukon, Canada in May 2016. Linear regression (LR) and simple kriging (SK), combined with cross correlation and Bayesian model averaging, are used to interpolate point-scale WB estimates. Snow distribution patterns differ considerably between glaciers, highlighting strong inter- and intra-basin variability. Elevation and a simple parameterization of wind redistribution are found to be the dominant controls of the spatial distribution of gridcell WB, but the relationship varies considerably between glaciers. Through a Monte Carlo analysis, we find that the interpolation of WB data is a larger source of uncertainty than the assignment of snow density or than the uncertainty in gridcell WB. For our study glaciers, the total WB uncertainty ranges from 0.03 m w.e. (8%) to 0.15 m w.e. (54%) depending primarily on the interpolation method. Despite the challenges associated with accurately and precisely estimating glacier-wide WB, our results are consistent with the previously reported regional WB gradient. (231 words)**

## INTRODUCTION

Winter surface mass balance, or "winter balance", is the net accumulation and ablation of snow over the winter season (Cogley and others, 2011), which constitutes glacier mass input. Accurate estimation of winter surface mass balance is critical for correctly simulating the summer and overall mass balance of a glacier (e.g. Hock, 2005). Effectively representing the spatial distribution of snow is also important for simulating snow and ice melt and modelling energy and mass exchange between the land and atmosphere, allowing for better monitoring of surface runoff and its downstream effects (e.g. Clark and others, 2011).

Winter balance (WB) is notoriously difficult to estimate. Snow distribution in alpine regions is highly variable with short correlation length scales (e.g. Anderton and others, 2004; Egli and others, 2011; Grunewald and others, 2010; Helbig and van Herwijnen, 2017; López-Moreno and others, 2011, 2013; Machguth and others, 2006; Marshall and others, 2006) and is influenced by dynamic interactions between the atmosphere and complex topography, operating on multiple spatial and temporal scales (e.g. Barry, 1992; Liston and Elder, 2006; Clark and others, 2011). Extensive, high resolution and accurate snow distribution measurements on glaciers are therefore almost impossible to achieve (e.g. Cogley and others, 2011; McGrath and others, 2015). Further, current models are

not able to fully represent these interactions so there is a significant source of uncertainty that undermines the ability of models to represent current and projected glacier conditions (Réveillet and others, 2016).

Those studies that have focused on obtaining detailed estimates of WB have used a wide range of measurement techniques, including direct measurement of snow depth and density (e.g. Cullen and others, 2017), lidar/photogrammerty (e.g. Sold and others, 2013) and ground penetrating radar (e.g. Machguth and others, 2006; Gusmeroli and others, 2014; McGrath and others, 2015). Spatial coverage of direct measurements is generally limited and often consists of an elevation transect along the glacier centreline (e.g. Kaser and others, 2003). Interpolation of these measurements is primarily done with a linear regression that includes only a few topographic parameters (e.g. MacDougall and Flowers, 2011), with elevation being the most common. Other established techniques include hand contouring (e.g. Tangborn and others, 1975), kriging (e.g. Hock and Jensen, 1999) and attributing measured accumulation values to elevation bands (e.g. Thibert and others, 2008). Physical snow models have been applied (e.g. Mott and others, 2008; Dadic and others, 2010) but a lack of detailed meteorological data generally prohibits their wide spread application. Error analysis is rarely undertaken and few studies have thoroughly investigated uncertainty in

spatially distributed estimates of winter balance estimates (c.f. Schuler and others, 2008).

More sophisticated models and measurement techniques of snow distribution are available and widely used in the field of snow science. Surveys described in the snow science literature are generally spatially extensive and designed to measure snow depth and density throughout a basin, ensuring that all terrain types are sampled. A wide array of measurement interpolation methods are used, including linear (e.g. López-Moreno and others, 2010) and non-linear regressions (e.g. Molotch and others, 2005) that include numerous terrain parameters, as well as geospatial interpolation (e.g. Erxleben and others, 2002) including various forms of kriging. Different interpolation methods are often combined (e.g. regression kriging) to yield improved fit (e.g. Balk and Elder, 2000). Physical snow models such as Alpine3D (Lehning and others, 2006) and SnowDrift3D (Schneiderbauer and Prokop, 2011) are widely used in snow science literature. Error analysis when estimating snow distribution has been examined from both a theoretical (e.g. Trujillo and Lehning, 2015) and applied perspective (e.g. Turcan and Loijens, 1975; Woo and Marsh, 1978; Deems and Painter, 2006).

The precision and accuracy of WB estimates can likely be improved by incorporating more sophisticated tools and interpolation methodologies, and by gaining a more comprehensive understanding of inherent uncertainties. The overall goals of our work are to (1) critically examine methods of moving from direct snow depth and density measurements to estimating WB and to (2) identify sources of uncertainty, evaluate their magnitude and assess their combined contribution to uncertainty in glacier-wide WB. We focus on commonly applied, low-complexity methods of measuring and estimating WB with the hope of making our results broadly applicable.

## STUDY SITE

Winter balance surveys were conducted on three glaciers in the Donjek Range of the St. Elias Mountains, located in south western Yukon, Canada (Fig. 1, Table 1). The Donjek Range is approximately $30 \times 30$ km and Glacier 4, Glacier 2 and Glacier 13 (labelling adopted from Crompton and Flowers (2016)) are located along a SW-NE transect through the range. These small, polythermal alpine glaciers are generally oriented SE-NW, with Glacier 4 predominantly southeast facing and Glaciers 2 and 13 generally northwest facing. The glaciers have simple geometries with steep head and valley walls.

The St. Elias Mountains rise sharply from the Pacific Ocean, creating a significant climatic gradient between coastal maritime conditions, generated by Aleutian–Gulf of Alaska low-pressure systems, and interior continental conditions, driven by the Yukon–Mackenzie high-pressure system (Taylor-Barge, 1969). The boarder between the two climatic zones is generally aliged with the divide between Hubbard and Kaskawulsh Glaciers, approximately 13 km from the ocean. The Donjek Range is located approximately 40 km to the east of the divide between the Hubbard and Kaskawulsh Glaciers (Taylor-Barge, 1969). Research on snow distribution and glacier mass balance in this area is limited. A series of research programs were operational in the 1960s (Wood, 1948; Danby and others, 2003) and long-term studies on a few alpine glaciers have arisen in the last 30 years (Flowers and others, 2014).

## METHODS

Estimating glacier-wide WB involves transforming measurements of snow depth and density into distributed gridcell-estimated WB. We do this in four steps: (1) We obtain direct measurements of snow depth and density in the field. (2) We interpolate density measurements to all depth-measurement locations in order to calculate the point-scale WB at each of these locations. This is necessary because we measure density at relatively few locations of depth. (3) We average all point-scale WBs within each gridcell of a digital elevation model (DEM) to obtain gricell-averaged WB. (4) We interpolate and extrapolate these gridcell-averaged WBs to obtain gridcell-estimated WB (in m w.e.) for each gridcell across the glacier surface. We choose to use a linear regression between gridcell-averaged WB and a number of topographic parameters because there is precedent for success (e.g. McGrath and others, 2015) and we use cross-validation and model averaging to test all combinations of these parameters. We also use simple kriging (SK), which is a data-driven interpolation method, to estimate gridcell-estimated WB without invoking physical interpretation (e.g. Hock and Jensen, 1999). The glacier-wide WB is then calculated by taking the integrated sum of gridcell-estimated WBs and dividing by the glacier area. For brevity, we refer to these four steps as (1) field measurements, (2) density assignment method, (3) gridcell-averaged WB and (4) distributed WB. Detailed methodology for each step is outlined below.

### Field measurements

*Sampling design*

The snow surveys were designed to capture variability in snow depth at regional, basin, gridcell and point scales (Clark and others, 2011). To capture variability at the regional scale we chose three glaciers along the precipitation gradient in the St. Elias Mountains, Yukon (Fig. 1b) (Taylor-Barge, 1969). To account for basin-scale variability, snow depth was measured along linear and curvilinear transects on each glacier (Fig. 1c) with sample spacing of $10 - 60$ m (Fig. 1d). Sample spacing was restricted by glacier travel and the need to complete surveys on all three glaciers within the period of peak accumulation. We selected centreline and transverse transects because they are commonly used for winter balance estimates (e.g. Kaser and others, 2003; Machguth and others, 2006) as well as an hourglass pattern with an inscribed circle, which allows for sampling in multiple directions and easy travel (Parr, C., 2016 personal communication). To capture variability at the gridcell scale, we densely sample up to four gridcells on each glacier using a linear-random sampling design termed 'zigzag'. To capture point-scale variability, we took 3–4 depth measurements within ~1 m of each other (Fig. 1e) at each transect measurement location. In total, we collected
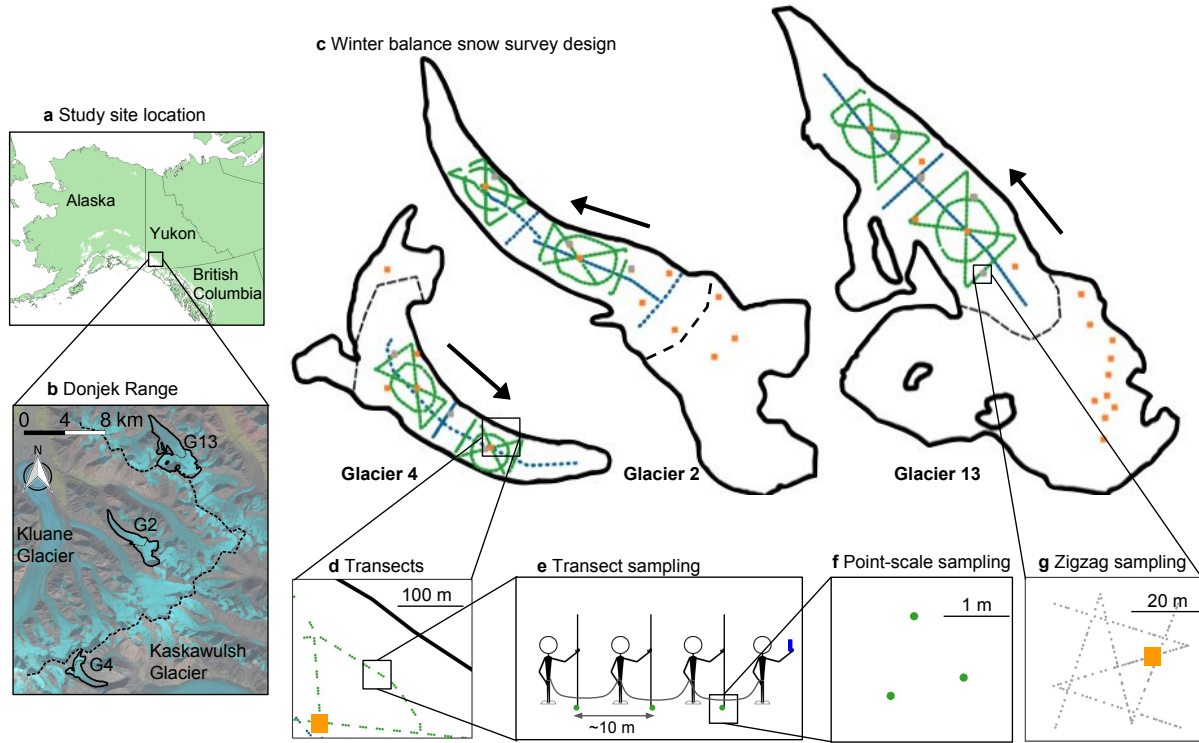
**Fig. 1.** Study area location and sampling design for Glaciers 4, 2 and 13. (a) The study region is located in the Donjek Range of the St. Elias Mountains of Yukon, Canada. (b) Study glaciers are located along a SW-NE transect through the Donjek Range. The local topographic divide is shown as a dashed line. Imagery from Landsat8 (5 September 2013, data available from the U.S. Geological Survey). (c) Details of the snow survey sampling design. Centreline and transverse transects are shown in blue dots, hourglass and circle design are shown in green dots. Orange squares are locations of snow density measurements. Arrows indicate glacier flow direction and the approximate location of each ELA is shown as a black dashed line. (d) Linear and curvilinear transects typically consist of sets of three measurement locations, (e) spaced ~10 m apart. (f) At each location, three snow-depth measurements are made. (f) Linear-random snow-depth measurements in 'zigzag' design are shown as grey dots.

more than 9000 snow depth measurements throughout the study area (Table 1).

### Snow depth: transects

WB can be estimated as the product of the snow depth and depth-averaged density. Snow depth is generally accepted to be more variable than density (Elder and others, 1991; Clark and others, 2011; López-Moreno and others, 2013) so we chose a sampling design that resulted in a ratio of approximately 55:1 snow depth to snow density measurements. Our sampling campaign involved four people and occurred between 5–15 May, 2016, which corresponds to the historical peak seasonal snow accumulation in Yukon (Yukon Snow Survey Bulletin and Water Supply Forecast, May 1, 2016). While roped-up for glacier travel at fixed distances between observers, the lead observer used a single-frequency GPS unit (Garmin GPSMAP 64s) to navigate between predefined transect measurement locations (Fig. 1e). The remaining three observers used 3.2 m graduated aluminium avalanche probes to make snow depth measurements. The location of each set of depth measurements, taken by the second, third and fourth observers, was approximated based on the recorded location of the first observer and the direction of travel.

Snow depth sampling was concentrated in the ablation area to ensure that only snow from the current accumulation season was measured. The boundary between snow and firn in the accumulation area can be difficult to detect and often misinterpreted, especially when using an avalanche probe (Grunewald and others, 2010; Sold and others, 2013). We intended to use a firn corer to measure WB in the accumulation area, but cold snow combined with positive air temperatures led to cores being unrecoverable. Successful snow depth and density measurements within the accumulation area were made either in snow pits or using a Federal Sampler to unambiguously identify the snow–firn transition.

### Snow depth: zigzags

To capture snow-depth variability within a single DEM gridcell, we implemented a linear-random sampling design (Shea and Jamieson, 2010), termed 'zigzag'. We measured depth at random intervals (0.3–3.0 m) along two 'Z'-shaped transects within three to four $40 \times 40$ m gridcells (Fig. 1g) resulting in 135–191 measurements in each zigzag. Zigzag locations were randomly chosen within the upper, middle, and lower portions of the ablation area of each glacier. We were able to measure a fourth zigzag on Glacier 13 that was located in the central ablation area (~2200 m a.s.l.).

**Table 1.** Physical characteristics of study glaciers and May 2016 winter balance survey details for Glacier 4 (G4), Glacier 2 (G2), and Glacier 13 (G13), including number of snow-depth measurement locations along transects ($n_T$), total length of transects ($d_T$), number of combined snow pit (SP) and Federal Sampler (FS) density measurement locations ($n_\rho$) and number of zigzag surveys ($n_{zz}$).

| | Location | Elevation (m a.s.l) | | | Slope (°) | Area | Date | Survey Details | | | |
|---|---|---|---|---|---|---|---|---|---|---|---|
| | UTM Zone 7 | *Mean* | *Range* | *ELA* | *Mean* | **(km)** | | $n_T$ | $d_T$ (km) | $n_\rho$ | $n_{zz}$ |
| **G4** | 595470 E 6740730 N | 2344 | 1958–2809 | ~2500 | 12.8 | 3.8 | 4–7 May 2016 | 649 | 13.1 | 10 | 3 |
| **G2** | 601160 E 6753785 N | 2495 | 1899–3103 | ~2500 | 13.0 | 7.0 | 8–11 May 2016 | 762 | 13.6 | 11 | 3 |
| **G13** | 604602 E 6763400 N | 2428 | 1923–3067 | ~2380 | 13.4 | 12.6 | 12–15 May 2016 | 941 | 18.1 | 20 | 4 |

*Snow density*

Snow density was measured using a wedge cutter in three snow pits on each glacier, as well as with a Federal Sampler. Within the snow pit (SP), we measured a vertical density profile by inserting a $5 \times 10 \times 10$ cm wedge-shaped cutter ($250\,\mathrm{cm}^3$) in 5 cm increments and then weighing the samples with a Presola 1000 g spring scale (e.g. Gray and Male, 1981; Fierz and others, 2009). Uncertainty in estimating density from SPs stems from incorrect assignment of density to layers that could not be sampled (i.e. ice lenses and hard layers). We attempt to quantify this uncertainty by varying three values: ice layer thickness by $\pm 1$ cm ($\leq 100\%$) of the recorded thickness, ice layer density between 700 and $900\,\mathrm{kg\,m}^{-3}$ and the density of layers identified as being too hard to sample (but not ice) between 600 and $700\,\mathrm{kg\,m}^{-3}$. When considering all three sources of uncertainty, the range of integrated density values is always less than 15% of the reference density. Density values for shallow pits that contain ice lenses are particularly sensitive to changes in prescribed density and ice lens thickness.

While SPs provide the most accurate measure of snow density, digging and sampling a snow pit is time and labour intensive. Therefore, a Federal Snow Sampler (FS) (Clyde, 1932), which directly measures depth-integrated snow water equivalent, was used to augment the SP measurements. A minimum of three FS measurements were taken at each of $7-19$ locations on each glacier and an additional eight FS measurements were co-located with each SP profile. Measurements for which the snow core length inside the FS was less than 90% of the snow depth were discarded. Density values at each measurement location were then averaged and error is taken to be the standard deviation of these measurements.

During the field campaign there were two small accumulation events. The first, on 6 May 2016, also involved high winds so accumulation could not be determined. The second, on 10 May 2016, resulted in 0.01 m w.e accumulation measured at one location on Glacier 2. Positive temperatures and clear skies occurred between 11–16 May 2016, which we suspect resulted in melt occurring on Glacier 13. The snow in the lower part of the ablation area of Glacier 13 was isothermal and showed clear signs of melt and metamorphosis. The total amount of accumulation and melt during the study period could not be estimated so no corrections were made.

**Table 2.** Eight methods used to estimate snow density at unmeasured locations for purpose of converting measured snow depth to point-scale WB.

| Method code | Source of measured snow density | | Density assignment method |
|---|---|---|---|
| | *Snow pit* | *Federal Sampler* | |
| S1 | ■ | | Mean of measurements |
| F1 | | ■ | across all glaciers |
| S2 | ■ | | Mean of measurements |
| F2 | | ■ | within a given glacier |
| S3 | ■ | | LR of density on elevation |
| F3 | | ■ | within a given glacier |
| S4 | ■ | | Inverse distance |
| F4 | | ■ | weighted mean |

## Density assignment method

Measured snow density must be interpolated or extrapolated to estimate point-scale WB at each snow-depth sampling location. We employ four, commonly used methods to interpolate density (Table 2): (1) calculating mean density over an entire mountain range (e.g. Cullen and others, 2017), (2) calculating mean density for each glacier (e.g. Elder and others, 1991; McGrath and others, 2015), (3) linear regression of density on elevation for each glacier (e.g. Elder and others, 1998; Molotch and others, 2005) and (4) inverse-distance weighted density (e.g. Molotch and others, 2005). SP- and FS-derived densities are treated separately, for reasons explained below, resulting in eight possible methods of assigning density.

## Gridcell-averaged winter balance

We average one to six (mean of 2.1 measurements) point-scale WBs within each $40 \times 40$ m DEM gridcell to obtain gricell-averaged WB. The locations of measurements have considerable uncertainty both from the error in the horizontal position given by the GPS unit (2.7–4.6 m) and the estimation of observer location based on the recorded GPS positions of the navigator. These errors could result in the incorrect assignment of a point-scale WB to a particular gridcell. However, this source of error is not further investigated because we assume that gridcell-averaged WB uncertainty is captured in the zigzag measurements described below. We are able to combine data from different observers because there are no significant differences between snow depth measurements made by

observers along a transect (p>0.05), with the exception of the first transect on Glacier 4.

## Distributed winter balance

### Linear regression

Gridcell-averaged WBs are interpolated and extrapolated across each glacier using linear regression (LR) as well as simple kriging (SK). We use LR to relate gridcell-averaged WB to gridcell values of DEM-derived topographic parameters. We chose the most commonly applied topographic parameters within WB studies (e.g. McGrath and others, 2015), which include elevation, slope, aspect, curvature, "northness" and a wind-redistribution parameter and add distance from centreline as an additional parameter to account for possible variability across the width of each glacier. Our sampling design ensured that the ranges of topographic parameters associated with our measurement locations represent more than 70% of the total area of each glacier (except for the elevation range on Glacier 2 which is 50%). Topographic parameters are weighted by a set of fitted regression coefficients ($\beta_i$) calculated by minimizing the sum of squares of the vertical deviations of each datum from the regression line (Davis and Sampson, 1986). For details on data and methods used to estimate the topographic parameters see the Supplementary Material.

To avoid overfitting the data and to encompass all possible combinations of topographic parameters, cross-validation and model averaging are implemented. First, cross-validation is used to obtain a set of $\beta_i$ values that have the greatest predictive ability. We randomly select 1000 subsets (2/3 of the values) of the data to fit the LR and the remaining data (1/3 of the values) are used to calculate a root mean squared error (RMSE) (Kohavi and others, 1995). Regression coefficients resulting in the lowest RMSE are selected. Second, we use model averaging to take into account uncertainty when selecting predictors and to also maximize predictive ability (Madigan and Raftery, 1994). Models are generated by calculating a set of $\beta_i$ for all possible combinations of predictors. Following a Bayesian framework, model averaging involves weighting all models by their posterior model probabilities (Raftery and others, 1997). To obtain the final regression coefficients, the $\beta_i$ values from each model are weighted according to the relative predictive success of the model, as assessed by the value of the Bayesian Information Criterion (BIC) (Burnham and Anderson, 2004). BIC penalizes more complex models which further reduces the risk of overfitting. Gridcell-estimated WB is then estimated by applying the resulting regression coefficients to the topographic parameters associated with each gridcell.

### Simple kriging

Simple kriging (SK) is a data-driven method of estimating values at unsampled locations by using the isotropic spatial correlation (covariance) of measured values to find a set of optimal weights (Davis and Sampson, 1986; Li and Heap, 2008). SK assumes spatial correlation between sampling points that are distributed across a surface and then applies the correlation to interpolate between sampling points. We used the `DiceKriging` R package (Roustant and others, 2012) to calculate the maximum likelihood covariance matrix, as well as range distance ($\theta$) and nugget for gridcell-averaged winter balance values. The range distance is a measure of data correlation length and the nugget is the residual that encompasses sampling-error variance as well as the spatial variance at distances less than the minimum sample spacing (Li and Heap, 2008). SK cannot be used to understand physical processes that may be controlling snow distribution and in the absence of data, cannot be used to estimate winter balance on an unmeasured, neighbouring glacier.

## Uncertainty analysis

To quantify the uncertainty on the estimated glacier-wide WB, we conduct a Monte Carlo analysis, which uses repeated random sampling of input variables to calculate a distribution of output variables (Metropolis and Ulam, 1949). This random sampling process is done 1000 times, resulting in a distribution of possible glacier-wide WB values based on uncertainties associated with the four steps outlined above. We use the standard deviation of the WB distribution as a useful metric of uncertainty of the glacier-wide WB. Three sources of uncertainty are considered separately: the uncertainty due to (1) averaging point-scale WBs within a gridcell ($\sigma_{GS}$), (2) density assignment method ($\sigma_\rho$) and (3) interpolating and extrapolating gridcell-averaged WBs ($\sigma_{INT}$). These individual sources of uncertainty are propagated through the conversion of snow depth and density measurements to glacier-wide WB. Finally, the cumulative effect of all three sources of uncertainty on the glacier-wide WB is quantified.

### Grid-scale uncertainty ($\sigma_{GS}$)

We make use of the grid-scale zigzag surveys to represent the uncertainty in averaging point-scale WB to obtain gridcell-averaged WBs. For simplicity, we assume the same grid-scale uncertainty between gridcells for each glacier and represent this uncertainty by a normal distribution. The normal distribution is centred at zero and has a standard deviation equal to the mean standard deviation of all zigzags on each glacier. For each iteration of the Monte Carlo, a set of WB values is randomly chosen from the distribution and added to the gridcell-averaged WBs. These perturbed gridcell-averaged WBs are then used in the interpolation. Uncertainty in glacier-wide WB due to grid-scale uncertainty ($\sigma_{GS}$) is represented as the standard deviation of the resulting distribution of glacier-wide WB estimates.

### Density assignment uncertainty ($\sigma_\rho$)

We incorporate uncertainty in density assignment method by carrying forward all eight density interpolation methods when estimating glacier-wide WB. Using multiple density interpolation methods results in a generous estimate of density assignment uncertainty because we use a broad spectrum of the density measurement and interpolation methods. The glacier-wide WB uncertainty due to density assignment uncertainty ($\sigma_\rho$) is calculated as the standard deviation of glacier-wide WB estimates calculated using each density assignment method.

*Interpolation uncertainty ($\sigma_{\mathrm{INT}}$)*

We represent the uncertainty due to interpolation of gridcell-averaged WBs in different ways for LR and SK. LR interpolation uncertainty is represented by a multivariate normal distribution of possible regression coefficients ($\beta_i$). The standard deviation of each distribution is calculated using the covariance of regression coefficients as outlined in Bagos and Adam (2015), which ensures that regression coefficients are internally consistent. The $\beta_i$ distributions are randomly sampled and used to calculate gridcell-estimated WB.

SK interpolation uncertainty is represented by the 95% confidence interval for gridcell-estimated WB generated by the `DiceKriging` package. From this confidence interval, the standard deviation of each gridcell-estimated WB is then calculated. The standard deviation of glacier-wide WB is then found by taking the square root of the average variance of each gridcell-estimated WB. The final distribution of glacier-wide WB values is centred at the SK glacier-wide WB estimate. For consistency, the standard deviation of glacier-wide WB values that result from either LR or SK interpolation uncertainty is referred to as $\sigma_{\mathrm{INT}}$.

## RESULTS AND DISCUSSION

### Field measurements

*Snow depth*

We observed a wide range of snow depth on all three study glaciers, with Glacier 4 having the highest mean snow depth and Glacier 13 having the lowest (Fig. 2). At each measurement location, the median range of measured depths ($3 - 4$ points) as a percent of the mean depth at that location is 2%, 11%, and 12%, for Glaciers 4, 2 and 13, respectively. While Glacier 4 has the lowest point-scale variability, it also has the highest proportion of outliers, indicating a more variable snow depth across the glacier. The average standard deviation of all zigzag WB measurements on Glacier 4 is 0.027 m w.e., on Glacier 2 is 0.035 m w.e. and on Glacier 13 is 0.040 m w.e. WB data for each zigzag are not normally distributed about the mean WB value (Fig. 3).

*Snow density*

Contrary to expectation, co-located FS and SP measurements are found to be uncorrelated ($R^2 = 0.25$, Fig. 2b). The FS appears to oversample in deep snow and undersample in shallow snow. Oversampling by small-diameter (3.2–3.8 cm) sampling tubes has been observed in previous studies, with a percent error between 6.8% and 11.8% (e.g. Work and others, 1965; Fames and others, 1982; Conger and McClung, 2009). Studies that use FSs often apply a 10% correction to all measurements for this reason (e.g. Molotch and others, 2005). Oversampling has been attributed to slots "shaving" snow into the tube as it is rotated (e.g. Dixon and Boon, 2012) and to snow falling into the slots, particularly for snow samples with densities $>400\,\mathrm{kg\,m^{-3}}$ and snow depths $>1\,\mathrm{m}$ (e.g. Beauont and Work, 1963). Undersampling is likely to occur due to snow falling out of the bottom of the sampler (Turcan and Loijens, 1975), which likely occurred in our study since a
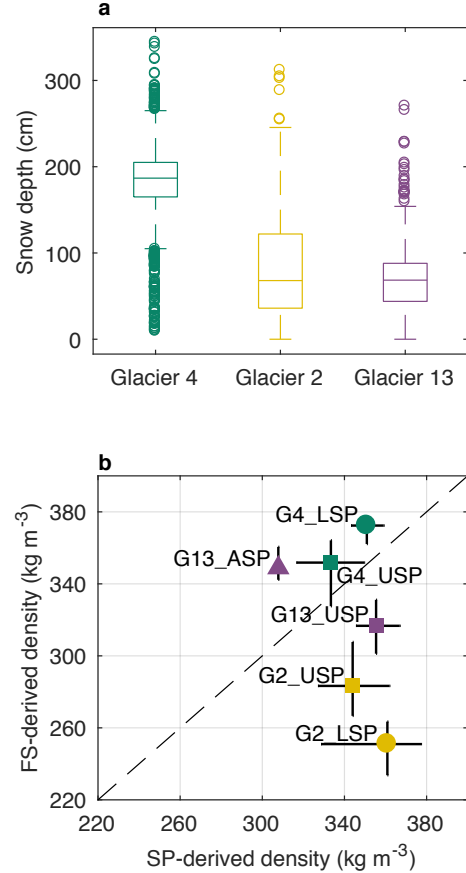


**Fig. 2.** Snow depth and density data. (a) Boxplot of measured snow depth on Glaciers 4, 2 and 13. The box shows first quartiles, the line within the box indicates the median, bars indicate minimum and maximum values (excluding outliers) and circles show outliers, which are defined as being outside of the range of 1.5 times the quartiles (approximately $\pm 2.7\sigma$). (b) Comparison of integrated density estimated using a vertical profile sampled in 5 cm increments using a wedge cutter in a snow pit (SP) and density estimated using Federal Sampler measurements (FS) for Glacier 4 (G4), Glacier 2 (G2) and Glacier 13 (G13). Labels indicate snow pit locations in the accumulation area (ASP), upper ablation area (USP) and lower ablation area (LSP). Error bars are determined differently for SP and FS densities (see text).

large portion of the lower elevation snow on both Glaciers 2 and 13 was isothermal, melt affected and weak, allowing for easier lateral displacement of the snow as the sampler was extracted. Relatively poor FS spring-scale sensitivity also made it difficult to obtain accurate measurements for snow depths <20 cm.

Additionally, FS density values are positively correlated with snow depth ($R^2 = 0.59$). This positive relationship could be a result of physical processes, such as compaction in deep snow and preferential formation of depth hoar in shallow snow, but is more likely a result of measurement artefacts for a number of reasons. First, the range of densities measured by the Federal Sampler is large (227–431 kg m$^{-3}$) and the extreme values seem unlikely given the conditions at the time of sampling within our study region,
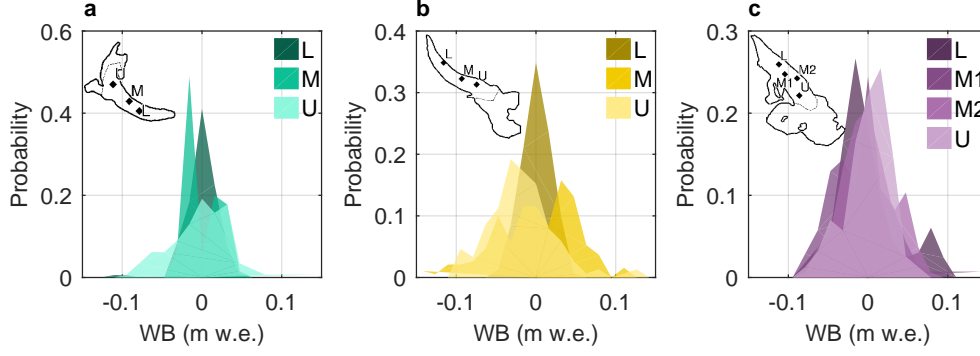
**Fig. 3.** Distributions of estimated SWE values for each zigzag survey. Local mean has been subtracted. (a) Glacier 4 zigzag surveys. (b) Glacier 2 zigzag surveys. (c) Glacier 13 zigzag surveys. Zigzag locations in lower (L), middle (M, M1, M2) and upper (U) ablation areas are shown in insets.

which experiences a continental snow pack with minimal mid-winter melt events. Second, compaction effects of a magnitude able of explaining density differences between SP and FS would not be expected at the measured depths (up to 340 cm). Third, no linear relationship exists between depth and SP-derived density ($R^2 = 0.05$). Together, these findings indicate that the FS measurements have a bias which is challenging to correct for.

## Density assignment method

Since we find no correlation between co-located SP and FS densities (Fig. 2), SP- and FS-derived densities are used separately (Table 2). SP-derived regional (S1) and glacier mean (S2) densities are within one standard deviation of FS-derived densities (F1 and F2) although SP-derived density values are larger (see Supplementary Material, Table 5). For both SP- and FS-deived densities, the mean of densities for any given glacier (S2 or F2 values) is within one standard deviation of the mean across all glaciers (S1 or F2 value). Correlations between elevation and SP- and FS-derived densities are generally high ($R^2 > 0.5$) but vary between glaciers and density measurement method (Supplementary material, Table 5). For any given glacier, the standard deviation of 3–4 SP-derived densities is <13% of the mean of those values (S2 values) (Supplementary material, Table 5). We adopt glacier-wide mean of SP-derived densities (S2) as the density assignment method for our reference case. This is consistent with most winter balance studies, which assume a uniform density for individual glaciers and measure snow density profiles at multiple locations in a study basin (e.g. Elder and others, 1991; McGrath and others, 2015; Cullen and others, 2017). Despite this, S2 density assignment method does not account for known basin-scale spatial variability in snow density (e.g. Wetlaufer and others, 2016).

## Gridcell-averaged winter balance

The distributions of gridcell-averaged WB for the individual glaciers are similar to those in Fig. 2a but with fewer outliers. The standard deviation of zigzag WB values is

**Table 3.** Glacier-wide winter balance (WB, m w.e.) estimated using linear regression and simple kriging for the three study glaciers. Root mean squared error (RMSE, m w.e.) is computed as the average of all RMSE values between gridcell-estimated WB and gridcell-averaged WBs that were randomly selected and excluded from interpolation (1/3 of all data). RMSE as a percent of the glacier-wide WB is shown in brackets.
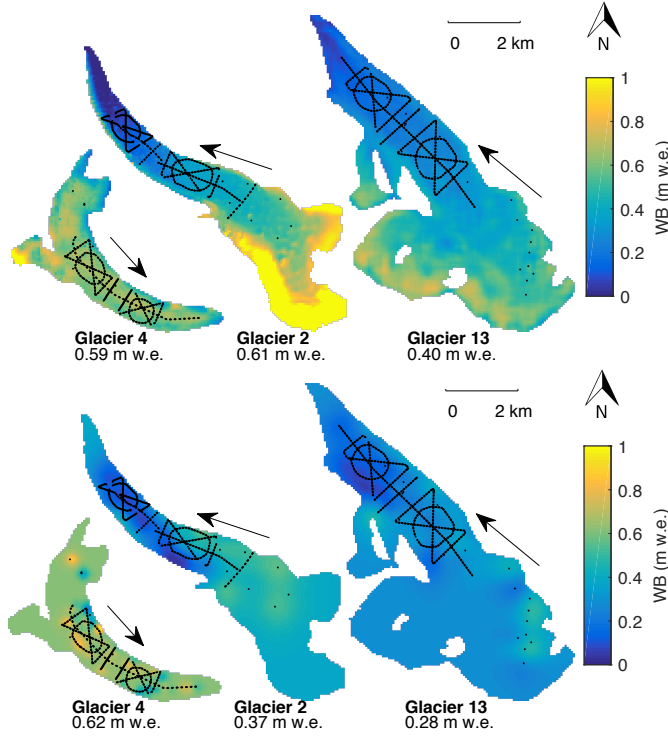
|  | Linear regression | | Simple kriging | |
| --- | --- | --- | --- | --- |
|  | WB | RMSE | WB | RMSE |
| **G4** | 0.582 | 0.153 (26%) | 0.616 | 0.134 (22%) |
| **G2** | 0.577 | 0.102 (18%) | 0.367 | 0.073 (20%) |
| **G13** | 0.381 | 0.080 (21%) | 0.271 | 0.068 (25%) |

almost twice as large as the mean standard deviation of point-scale WB values within a gridcell measured along transects. However, a small number of gridcells sampled in transect surveys have standard deviations in WB that exceed 0.25 m w.e. We nevertheless assume that the gridcell uncertainty is captured with dense sampling in zigzag gridcells. As a result, there is little need to take multiple measurements within a gridcell along a transect meaning that along-track transect spacing can be decreased to allow for greater spatial coverage of transects.
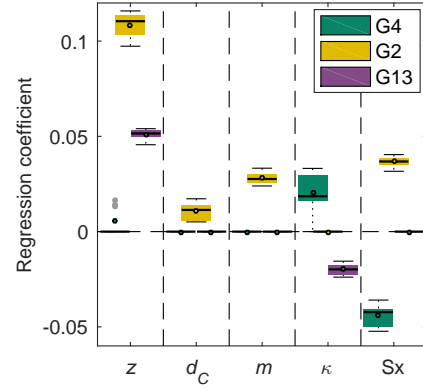
## Distributed winter balance

### Linear Regression

Analysis of topographic parameters reveals that elevation ($z$) is the most significant predictor of gridcell-averaged WB for Glaciers 2 and 13, while wind distribution ($Sx$) is the most significant predictor for Glacier 4 (Fig. 5). Gridcell-averaged WB is positively correlated with elevation. It is possible that the elevation correlation was accentuated due to melt onset (1–2 week early), especially on Glacier 13 (Yukon Snow Survey Bulletin and Water Supply Forecast, May 1, 2016). The southwestern Yukon winter snow pack in 2016 was also well below average (Yukon Snow Survey Bulletin and Water Supply Forecast, May 1, 2016), possibly emphasizing effects of early melt onset. Many WB studies have found elevation to be the most significant predictor

**Fig. 4.** Spatial distribution of gridcell-estimated winter balance (WB) found using linear regression (top row) and simple kriging (bottom row). Locations of point-scale WB values are shown as black dots. Gridcell-averaged WB values are calculated using glacier-wide mean SP-derived densities (S2, Table 2). Glacier flow directions are indicated by arrows. Values of glacier-wide WB are given below labels.



**Fig. 5.** Distribution of coefficients determined by linear regression of gridcell-averaged WB on gridcell topographic parameters for the eight different density assignment methods (Table 2) on each study glaciers. Coefficients are calculated using normalized data resulting in directly comparable coefficient values. Regression coefficients that are not significant are assigned a value of zero. Topographic parameters include elevation ($z$), distance from centreline ($d_C$), slope ($m$), curvature ($\kappa$) and wind exposure ($Sx$). Aspect ($\alpha$) and "northness" ($N$) are not shown because coefficient values are zero for all interpolation methods. The box shows first quartiles, the line within the box indicates the median, circle within the box indicated mean, bars indicate minimum and maximum values (excluding outliers) and gray dots show outliers, which are defined as being outside of the range of 1.5 times the quartiles (approximately $\pm 2.7\sigma$).

of WB data (e.g. Machguth and others, 2006; McGrath and others, 2015). However, WB–elevation gradients vary considerably between glaciers (e.g. Winther and others, 1998) and other factors, such as glacier orientation relative to dominant wind direction and glacier shape, have been noted to affect WB distribution (Machguth and others, 2006; Grabiec and others, 2011). There are also a number of studies that find no significant correlation between WB on glaciers and topographic parameters, with highly variable distribution of snow attributed to complex interactions between topography and the atmosphere (e.g. Grabiec and others, 2011; López-Moreno and others, 2011). Linearly extrapolating relationships into unmeasured locations, especially the accumulation area, is most susceptible to large errors (Fig. 7). The accumulation area typically also has the highest WB (Fig. 4), affecting the glacier-wide WB estimated for the glacier. In our study, the dependence of WB on elevation results in ∼1% of the area of Glacier 2 with gridcell-estimated WB >1.5 m w.e.

Gridcell-averaged WB is negatively correlated with $Sx$ on Glacier 4, counter-intuitively indicating less snow in 'sheltered' areas, while gridcell-averaged WB is positively correlated with $Sx$ on Glaciers 2 and 13. Similarly, gridcell-averaged WB is positively correlated with curvature for Glacier 4 and negatively correlated for the other two glaciers. Wind redistribution and preferential deposition of

snow is known to have a large influence on accumulation at sub-basin scales (e.g. Dadic and others, 2010; Winstral and others, 2013; Gerber and others, 2017). Our results indicate that wind likely has an impact on snow distribution but that the wind redistribution parameter may not adequately represent wind effects as applied to our study glaciers. For example, Glacier 4 is located in a curved valley with steep side walls, so specifying a single cardinal direction for wind may not be adequate. Further, the scale of deposition may be smaller than the resolution of the $Sx$ parameter estimated from our DEM. Our results corroborate McGrath and others (2015), who undertook a WB study on six glaciers in Alaska (DEM resolutions of 5 m) and found that $Sx$ was the only other significant parameter, besides elevation, for all glaciers. $Sx$ regression coefficients were smaller than elevation regression coefficients and in some cases, negative. Sublimation from blowing snow has also been shown to be an important mechanism mass loss from ridges (e.g. Musselman and others, 2015). Incorporating snow loss, as well as redistribution and preferential deposition, may be needed for accurate representations of distributed WB.

While LRs have been used to predict WB in other basins, we find that transfer of LR coefficients between glaciers results in large estimation error. The lowest root mean squared error (0.21 m w.e.) results from estimating a LR
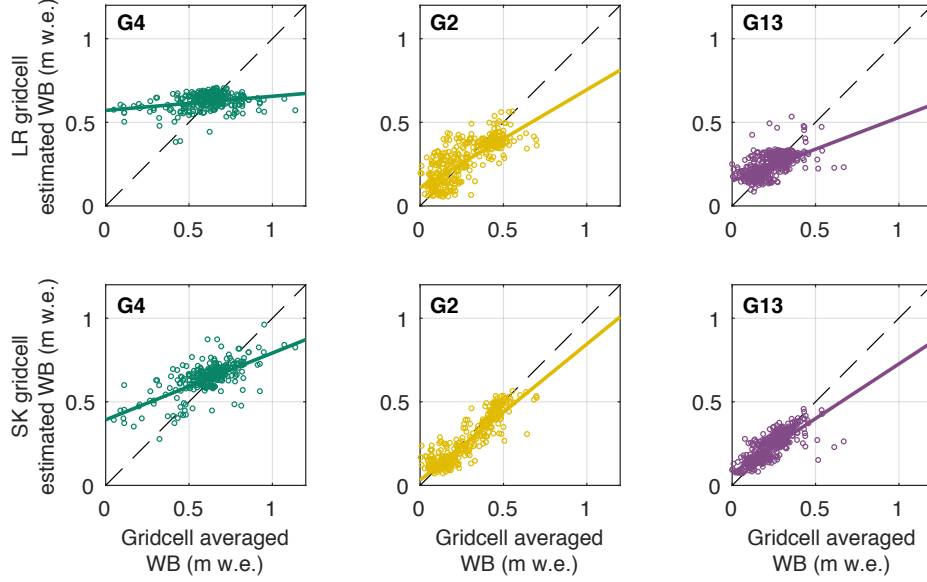
**Fig. 6.** Estimated winter balance (WB) versus WB data. Gridcell-estimated WB is found using linear regression (LR, top row) and simple kriging (SK, bottom row) and is plotted against gridcell-averaged WB along with best fit regression lines for Glacier 4 (left), Glacier 2 (middle) and Glacier 13 (right).

using all available observations. Our results are consistent with Grünewald and others (2013), who found that local statistical models are able to perform relatively well but they cannot be transferred to different basins and that regional-scale models are not able to explain the majority of observed variance.

*Simple kriging*

Since simple kriging (SK) is a data-driven interpolation method, the RMSE of gridcell-estimated WB values is lower for SK than LR (Fig. 6 and Table 3). However, the uncertainty in glacier-wide WB that arises from using SK is large, and unrealistic glacier-wide WBs of 0 m w.e. can be estimated. Further, our observations are generally limited to the ablation area, so SK produces almost uniform gridcell-estimated WBs in the accumulation area, which is inconsistent with observations described in the literature (e.g. Machguth and others, 2006; Grabiec and others, 2011). Extrapolation using SK leads to large uncertainty (Fig. 7) in estimating WB, further emphasizing the need for spatially distributed point-scale WB measurements in a glacierized basin.

Fitted kriging parameters, including the nugget and spatial correlation length, can provide insight into important scales of WB variability. Glaciers 2 and 13 have longer correlation lengths ($\sim$450 m) and smaller nuggets, indicating variability at larger scales (see Supplementary Material Table 6). Conversely, the model fitted to the SWE data for Glacier 4 has a short correlation length (90 m) and large nugget, indicating that accumulation variability occurs at smaller scales.

*LR and SK comparison*

LR and SK estimate a winter balance of $\sim$0.6 m w.e. for Glacier 4 but both are poor predictors of gridcell-averaged WB at measurement locations (Table 3). For Glaciers 2 and 13, SK estimates are more than 0.1 m w.e. (up to 40%) lower than LR estimates (Table 3) due to differences in extrapolation. Gridcell-estimated WBs found using LR and SK differ considerably in the upper accumulation areas of Glaciers 2 and 13 (Fig. 4), where observations are sparse and topographic parameters, like elevation, vary dramatically. The significant influence of elevation in the LR results in substantially higher gridcell-estimated WBs at high elevation, whereas gridcell-estimated WBs found using SK approximate the mean of WB data in these areas. However, when only the ablation area is considered, LR and SK produce gridcell-estimated WBs that differ by less than 7% for all glaciers. Choice of interpolation method therefore affects how WB data is extrapolated, which has a large effect on glacier-wide WB estimates on our study glaciers.

## Uncertainty analysis

Glacier-wide WB is affected by uncertainty introduced when averaging point-scale WBs ($\sigma_{GS}$), when chosing a density assignment method ($\sigma_\rho$), and when interpolating WB data ($\sigma_{INT}$). We find that when using LR and SK, $\sigma_{INT}$ has a larger effect on WB uncertainty than $\sigma_{GS}$ or $\sigma_\rho$. In other words, the distribution of glacier-wide WBs that arises from $\sigma_{GS}$ is much narrower than the distribution that arises from $\sigma_{INT}$ (Fig. 8 and Table 4). The WB distributions obtained using LR and SK overlap for each glacier, but the distribution modes differ (Fig. 8). SK generally estimates lower WB in the accumulation area, which lowers the glacier-wide WB estimate. Our results
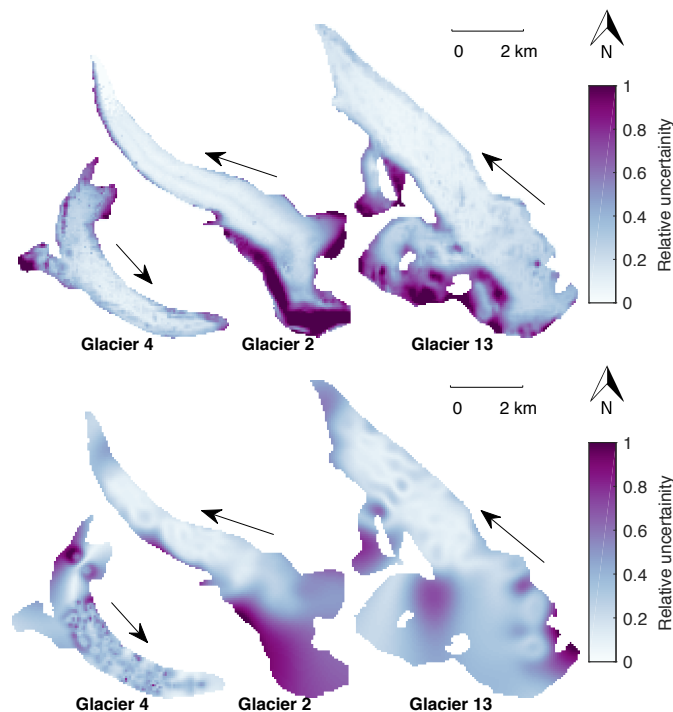
**Fig. 7.** Relative uncertainty in gridcell-estimated winter balance (WB) estimated using linear regression (top row) and simple kriging (bottom row). Relative uncertainty is calculated as the sum of differences between every pair of one hundred estimates of gridcell-estimated WB that include grid-scale and interpolation uncertainty. The sum is then normalized for each glacier. Values closer to one indicate higher relative uncertainty. Results for density interpolation method S2 are shown. Glacier flow directions are indicated by arrows.

caution against using extrapolated data to compare with WB estimates from remote sensing or modelling studies because this may produce misleading results. If possible, comparison studies should use point-scale WB data rather than interpolated WB values. For both LR and SK, the greatest uncertainty in gridcell-estimated WB occurs in the accumulation area (Fig. 7).

Grid-scale uncertainty ($\sigma_{GS}$) is the smallest contributor to WB uncertainty. This result is likely due to the fact that many parts of a glacier are characterized by a relatively smooth surface, with roughness lengths on the order of centimetres (e.g. Hock, 2005). Low WB uncertainty arising from $\sigma_{GS}$ implies that obtaining the most accurate value of gridcell-averaged WB does not need to be a priority when designing a snow survey. However, we assume that the gridcells selected for zigzag surveys are representative of $\sigma_{GS}$ across each glacier, which is likely not true for areas with debris cover, crevasses and steep slopes.

Our Monte Carlo analysis did not include uncertainty arising from a number of data sources, which we assume to be encompassed by investigated sources of uncertainty or to contribute negligibly to WB uncertainty. These neglected sources of uncertainty include error associated with SP and FS density measurement, DEM vertical and horizontal error and error associated with estimating measurement locations.

## Context and caveats

### Regional winter balance gradient

The glacier-wide WBs of our three study glaciers (S2 density assignment method), with an uncertainty equal to one standard deviation of the distribution found with Monte Carlo analysis, are: $0.593 \pm 0.029$ m w.e. on Glacier 4, $0.608 \pm 0.049$ m w.e. on Glacier 2 and $0.404 \pm 0.029$ m w.e. on Glacier 13. Although we find considerable inter- and intra-basin variability in WB estimates, our data are consistent with a regional-scale WB gradient for the continental side of the St. Elias Mountains (Fig. 9). WB data are compiled from Taylor-Barge (1969), the three glaciers presented in this paper, as well as two snow pits we dug near the head of the Kaskawulsh Glacier in May 2016. The data show a linear decrease $(-0.024$ m w.e. km$^{-1}$, R$^2$ =0.85) in WB with distance from the regional topographic divide between Kaskawulsh and Hubbard Glaciers in the St. Elias Mountains, as identified by Taylor-Barge (1969). While the three study glaciers fit the regional relationship, the same relationship would not apply if just the Donjek Range is considered. We infer that interaction between meso-scale weather patterns and large-scale mountain topography is a major driver of regional-scale WB. Further insight into regional-scale WB trends can be gained by investigating moisture source trajectories and the contribution of orographic precipitation to WB across the St. Elias Mountains.

### Limitations and future work

Extensions to this work could include investigating experimental design, examining the effects of DEM gridcell size on winter balance and resolving temporal variability. Our sampling design was chosen to extensively sample the ablation area and is likely too finely resolved for many future mass balance surveys to replicate. Determining a sampling design that minimizes error and reduces the number of measurements, known as data efficiency thresholds, would contribute to optimizing snow surveys in mountainous regions. For example, López-Moreno and others (2010) concluded that $200-400$ observations are needed to obtain accurate and robust snow distribution models within a non-glacierized alpine basin.

DEM gridcell size is known to significantly affect computed topographic parameters and the ability for a DEM to resolve important hydrological features (i.e. drainage pathways) in the landscape (Zhang and Montgomery, 1994; Garbrecht and Martz, 1994; Guo-an and others, 2001; López-Moreno and others, 2010), which can have implications when using topographic parameters in a LR. Zhang and Montgomery (1994) found that a 10 m gridcell size is an optimal compromise between resolution and data volume. Further, the relationship between topographic parameters and WB data is correlated with DEM gridcell size, whereby a decrease in spatial resolution of the DEM results in a decrease in the importance of curvature and an increase in the importance of elevation (e.g. Kienzle, 2004; López-Moreno and others, 2010). A detailed and
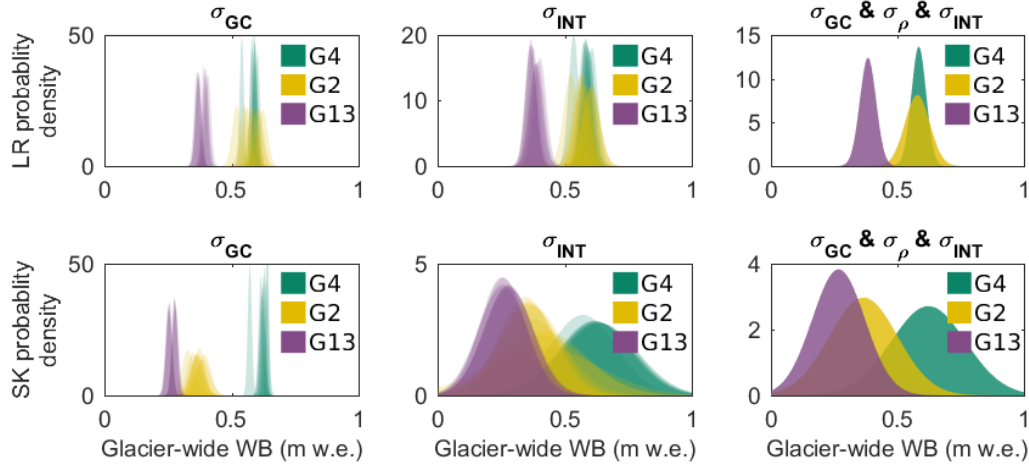
**Fig. 8.** Distributions of glacier-wide winter balance (WB) that arise from various sources of uncertainty. (Left column) WB distribution arising from grid-scale uncertainty ($\sigma_{GS}$). (Middle column) WB distribution arising from interpolation uncertainty ($\sigma_{INT}$). (Right column) WB distribution arising from a combination of $\sigma_{GS}$, $\sigma_{INT}$ and density assignment uncertainty ($\sigma_\rho$). Results are shown for interpolation by (top row) linear regression and (bottom row) simple kriging. Distributions for each density assignment method are plotted within each panel for Glacier 4 (G4), Glacier 2 (G2) and Glacier 13 (G13).
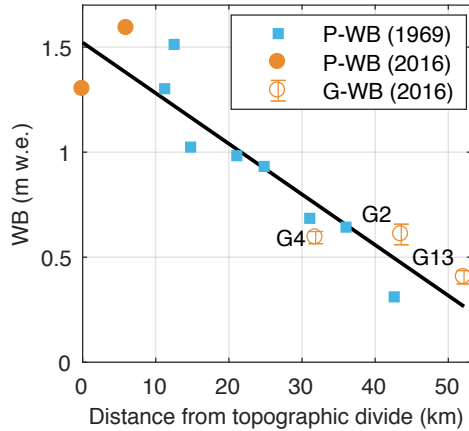


**Fig. 9.** Relation between winter balance (WB) and linear distance from the regional topographic divide between Kaskawulsh and Hubbard Glaciers in the St. Elias Mountains. Blue squares are point-scale WBs from snow-pit data reported by Taylor-Barge (1969). Open orange circles, labelled G4, G2 and G13, are glacier-wide WBs estimated with LR and density assignment S2 for Glaciers 4, 2 and 13, with errors bars calculated as the standard deviation of Monte Carlo-derived WB distributions (this study). Filled orange dots are point-scale WBs from snow-pit data at two locations in the accumulation area of the Kaskawulsh Glacier, collected in May 2016 (unpublished data, SFU Glaciology Group). Black line indicates line of best fit ($R^2 = 0.85$).

ground controlled DEM is therefore needed to accurately identify features that drive basin-scale WB. Even with a high resolution DEM, small-scale snow variability created by microtopography cannot be resolved. For example, the lower part of Glacier 2 has an undulating ice surface (5 m horizontal displacement and 0.5 m vertical displacement) that results in large variability in snow depth.

Temporal variability in accumulation is not considered in our study. While this limits our conclusions, a number of studies have found temporal stability in spatial patterns of snow accumulation and that terrain-based model could be applied reliable between years (e.g. Grünewald and others, 2013). For example, Walmsley (2015) analyzed more than 40 years of accumulation recorded on two Norwegian glaciers and found that snow accumulation is spatially heterogeneous yet exhibits robust time stability in its distribution.

## CONCLUSION

We estimate winter balance (WB) at various scales for three glaciers (termed as Glacier 2, Glacier 4 and Glacier 13) in the St. Elias Mountains from direct snow depth and density sampling. Our objectives are to (1) critically examine methods of moving from direct snow depth and density measurements to estimating WB and to (2) identify sources of uncertainty, evaluate their magnitude and assess their combined contribution to uncertainty in WB.

We find that interpolating and extrapolating gridcell-averaged WB has a large effect on glacier-wide WB. On Glacier 4, glacier-wide WB is consistent between linear regression (LR) and simple kriging (SK) but both explain only a small portion of the observed variance. This highlights that relatively precise glacier-wide WBs may not necessarily be accurate estimates. On Glaciers 2 and 13, LR and SK are better able to estimate gridcell-

**Table 4.** Standard deviation ($\times 10^{-2}$ m w.e.) of glacier-wide winter balance distributions arising from uncertainties in gridcell-averaged WB ($\sigma_{\mathrm{GS}}$), density assignment ($\sigma_\rho$), interpolation ($\sigma_{\mathrm{INT}}$) and all three sources combined ($\sigma_{\mathrm{ALL}}$) for linear regression (left columns) and simple kriging (right columns)

| | Linear regression | | | | Simple kriging | | | |
|---|---|---|---|---|---|---|---|---|
| | $\sigma_{\mathrm{GS}}$ | $\sigma_\rho$ | $\sigma_{INT}$ | $\sigma_{ALL}$ | $\sigma_{\mathrm{GS}}$ | $\sigma_\rho$ | $\sigma_{INT}$ | $\sigma_{ALL}$ |
| **Glacier 4** | 0.86 | 1.90 | 2.13 | 2.90 | 0.85 | 2.15 | 14.05 | 14.72 |
| **Glacier 2** | 1.80 | 3.37 | 3.09 | 4.90 | 2.53 | 2.03 | 13.78 | 13.44 |
| **Glacier 13** | 1.12 | 1.68 | 2.80 | 3.20 | 1.15 | 1.27 | 9.65 | 10.43 |

averaged WBs but glacier-wide WBs differ considerably between the two interpolation methods due to extrapolation into the accumulation area. Snow distribution patterns are found to differ considerably between glaciers, highlighting strong intra- and inter-basin variability and accumulation drivers acting on multiple scales. Gridcell-averaged WB on Glacier 4 is highly variable, as indicated by shorter range distance, higher nugget value and lower explained variance of gridcell-estimated WB. Glaciers 2 and 13 have lower gridcell-averaged WB variability and elevation is the primary control of observed variation.

For our study glaciers, the glacier-wide WB uncertainty ranges from 0.03 m w.e (8%) to 0.15 m w.e (54%), depending primarily on the interpolation method. Uncertainty within the interpolation method is the largest source of glacier-wide WB uncertainty when compared to uncertainty in grid-scale WB values and density assignment method. Future studies could reduce WB uncertainty by increasing the spatial distribution of snow depth sampling rather than the number of measurements within a single gridcell along a transect. In our work, increased sampling within the accumulation area would better constrain WB data extrapolation and decrease uncertainty. Despite challenges in accurately estimating WB, our data are consistent with a regional-scale WB gradient for the continental side of the St. Elias Mountains.

## References

Anderton S, White S and Alvera B (2004) Evaluation of spatial variability in snow water equivalent for a high mountain catchment. *Hydrological Processes*, **18**(3), 435–453 (doi: 10.1002/hyp.1319)

Bagos PG and Adam M (2015) On the Covariance of Regression Coefficients. *Open Journal of Statistics*, **5**(07), 680 (doi: 10.4236/ojs.2015.57069)

Balk B and Elder K (2000) Combining binary decision tree and geostatistical methods to estimate snow distribution in a mountain watershed. *Water Resources Research*, **36**(1), 13–26 (doi: 10.1029/1999WR900251)

Barry RG (1992) *Mountain weather and climate*. Psychology Press

Beauont RT and Work RA (1963) Snow sampling results from three sampler. *International Association of Scientific Hydrology. Bulletin*, **8**(4), 74–78 (doi: 10.1080/02626666309493359)

Berthier E, Arnaud Y, Kumar R, Ahmad S, Wagnon P and Chevallier P (2007) Remote sensing estimates of glacier mass balances in the Himachal Pradesh (Western Himalaya, India). *Remote Sensing of Environment*, **108**(3), 327–338

Burnham KP and Anderson DR (2004) Multimodel Inference: Understanding AIC and BIC in Model Selection. *Sociological Methods & Research*, **33**(2), 261–304 (doi: 10.1177/0049124104268644)

Clark MP, Hendrikx J, Slater AG, Kavetski D, Anderson B, Cullen NJ, Kerr T, Örn Hreinsson E and Woods RA (2011) Representing spatial variability of snow water equivalent in hydrologic and land-surface models: A review. *Water Resources Research*, **47**(7) (doi: 10.1029/2011WR010745)

Clyde GD (1932) Circular No. 99-Utah Snow Sampler and Scales for Measuring Water Content of Snow

Cogley J, Hock R, Rasmussen L, Arendt A, Bauder A, Braithwaite R, Jansson P, Kaser G, Möller M, Nicholson L and others (2011) Glossary of glacier mass balance and related terms

Conger SM and McClung DM (2009) Comparison of density cutters for snow profile observations. *Journal of Glaciology*, **55**(189), 163–169

Crompton JW and Flowers GE (2016) Correlations of suspended sediment size with bedrock lithology and glacier dynamics. *Annals of Glaciology*, 1–9 (doi: 10.1017/aog.2016.6)

Cullen NJ, Anderson B, Sirguey P, Stumm D, Mackintosh A, Conway JP, Horgan HJ, Dadic R, Fitzsimons SJ and Lorrey A (2017) An 11-year record of mass balance of Brewster Glacier, New Zealand, determined using a geostatistical approach. *Journal of Glaciology*, **63**(238), 199–217 (doi: 10.1017/jog.2016.128)

Dadic R, Mott R, Lehning M and Burlando P (2010) Parameterization for wind-induced preferential deposition of snow. *Journal of Geophysical Research: Earth Surface (2003–2012)*, **115** (doi: 10.1029/2009JF001261)

Danby RK, Hik DS, Slocombe DS and Williams A (2003) Science and the St. Elias: an evolving framework for sustainability in North America's highest mountains. *The Geographical Journal*, **169**(3), 191–204 (doi: 10.1111/1475-4959.00084)

Davis JC and Sampson RJ (1986) *Statistics and data analysis in geology*, volume 646. Wiley New York et al.

Deems JS and Painter TH (2006) Lidar measurement of snow depth: accuracy and error sources. In *Proceedings of the International Snow Science Workshop*, 1–6

Dixon D and Boon S (2012) Comparison of the SnowHydro snow sampler with existing snow tube designs. *Hydrological Processes*, **26**(17), 2555–2562, ISSN 1099-1085 (doi: 10.1002/hyp.9317)

Egli L, Griessinger N and Jonas T (2011) Seasonal development of spatial snow-depth variability across

different scales in the Swiss Alps. *Annals of Glaciology*, **52**(58), 216–222 (doi: 10.3189/172756411797252211)

Elder K, Dozier J and Michaelsen J (1991) Snow accumulation and distribution in an alpine watershed. *Water Resources Research*, **27**(7), 1541–1552 (doi: 10.1029/91WR00506)

Elder K, Rosenthal W and Davis RE (1998) Estimating the spatial distribution of snow water equivalence in a montane watershed. *Hydrological Processes*, **12**(1011), 1793–1808 (doi: 10.1002/(SICI)1099-1085(199808/09)12:10/11¡1793::AID-HYP695¿3.0.CO;2-)

Erxleben J, Elder K and Davis R (2002) Comparison of spatial interpolation methods for estimating snow distribution in the Colorado Rocky Mountains. *Hydrological Processes*, **16**(18), 3627–3649 (doi: 10.1002/hyp.1239)

Fames PE, Peterson N, Goodison B and Richards RP (1982) Metrication of Manual Snow Sampling Equipment. In *Proceedings of the 50th Western Snow Conference*, 120–132

Fierz C, Armstrong RL, Durand Y, Etchevers P, Greene E, McClung DM, Nishimura K, Satyawali PK and Sokratov SA (2009) *The international classification for seasonal snow on the ground*, volume 25. UNESCO/IHP Paris

Flowers GE, Copland L and Schoof CG (2014) Contemporary Glacier Processes and Global Change: Recent Observations from Kaskawulsh Glacier and the Donjek Range, St. Elias Mountains. *Arctic*, **67**, 22–34, copyright - Copyright Arctic Institute of North America 2014; Document feature - Maps; Illustrations; Graphs; ; Last updated - 2015-04-07

Garbrecht J and Martz L (1994) Grid size dependency of parameters extracted from digital elevation models. *Computers & Geosciences*, **20**(1), 85–87, ISSN 0098-3004 (doi: 10.1016/0098-3004(94)90098-1)

Gerber F, Lehning M, Hoch SW and Mott R (2017) A close-ridge small-scale atmospheric flow field and its influence on snow accumulation. *Journal of Geophysical Research: Atmospheres*, n/a–n/a, ISSN 2169-8996 (doi: 10.1002/2016JD026258), 2016JD026258

Grabiec M, Puczko D, Budzik T and Gajek G (2011) Snow distribution patterns on Svalbard glaciers derived from radio-echo soundings. *Polish Polar Research*, **32**(4), 393–421 (doi: 10.2478/v10183-011-0026-4)

Gray DM and Male DH (1981) *Handbook of snow: principles, processes, management & use*. Pergamon Press

Grunewald T, Schirmer M, Mott R and Lehning M (2010) Spatial and temporal variability of snow depth and ablation rates in a small mountain catchment. *Cryosphere*, **4**(2), 215–225 (doi: 10.5194/tc-4-215-2010)

Grünewald T, Stötter J, Pomeroy J, Dadic R, Moreno Baños I, Marturià J, Spross M, Hopkinson C, Burlando P and Lehning M (2013) Statistical modelling of the snow depth distribution in open alpine terrain. *Hydrology and Earth System Sciences*, **17**(8), 3005–3021 (doi: 10.5194/hess-17-3005-2013)

Guo-an T, Yang-he H, Strobl J and Wang-qing L (2001) The impact of resolution on the accuracy of hydrologic data derived from DEMs. *Journal of Geograph-ical Sciences*, **11**(4), 393–401, ISSN 1861-9568 (doi: 10.1007/BF02837966)

Gusmeroli A, Wolken GJ and Arendt AA (2014) Helicopter-borne radar imaging of snow cover on and around glaciers in Alaska. *Annals of Glaciology*, **55**(67), 78–88 (doi: 10.3189/2014AoG67A029)

Helbig N and van Herwijnen A (2017) Subgrid parameterization for snow depth over mountainous terrain from flat field snow depth. *Water Resources Research*, **53**(2), 1444–1456, ISSN 0043-1397 (doi: 10.1002/2016WR019872)

Hock R (2005) Glacier melt: a review of processes and their modelling. *Progress in Physical Geography*, **29**(3), 362–391 (doi: 10.1191/0309133305pp453ra)

Hock R and Jensen H (1999) Application of kriging interpolation for glacier mass balance computations. *Geografiska Annaler: Series A, Physical Geography*, **81**(4), 611–619 (doi: 10.1111/1468-0459.00089)

Kaser G, Fountain A, Jansson P and others (2003) *A manual for monitoring the mass balance of mountain glaciers*. Unesco Paris

Kienzle S (2004) The Effect of DEM Raster Resolution on First Order, Second Order and Compound Terrain Derivatives. *Transactions in GIS*, **8**(1), 83–111, ISSN 1467-9671 (doi: 10.1111/j.1467-9671.2004.00169.x)

Kohavi R and others (1995) A study of cross-validation and bootstrap for accuracy estimation and model selection. In *Proceedings of the Fourteenth International Joint Conference on Artificial Intelligence*, volume 14, 1137–1145

Korona J, Berthier E, Bernard M, Rémy F and Thouvenot E (2009) SPIRIT SPOT 5 stereoscopic survey of Polar Ice: Reference images and topographies during the fourth International Polar Year (2007–2009). *ISPRS Journal of Photogrammetry and Remote Sensing*, **64**(2), 204–212

Lehning M, Völksch I, Gustafsson D, Nguyen TA, Stähli M and Zappa M (2006) ALPINE3D: a detailed model of mountain surface processes and its application to snow hydrology. *Hydrological processes*, **20**(10), 2111–2128

Li J and Heap AD (2008) A review of spatial interpolation methods for environmental scientists No. Record 2008/23. *Geoscience Australia*

Liston GE and Elder K (2006) A distributed snow-evolution modeling system (SnowModel). *Journal of Hydrometeorology*, **7**(6), 1259–1276 (doi: 10.1175/JHM548.1)

López-Moreno J, Latron J and Lehmann A (2010) Effects of sample and grid size on the accuracy and stability of regression-based snow interpolation methods. *Hydrological Processes*, **24**(14), 1914–1928, ISSN 1099-1085 (doi: 10.1002/hyp.7564)

López-Moreno J, Fassnacht S, Heath J, Musselman K, Revuelto J, Latron J, Morán-Tejeda E and Jonas T (2013) Small scale spatial variability of snow density and depth over complex alpine terrain: Implications for estimating snow water equivalent. *Advances in Water Resources*, **55**, 40–52, ISSN 0309-1708 (doi: 10.1016/j.advwatres.2012.08.010), snow–Atmosphere Interactions and Hydrological Consequences

López-Moreno JI, Fassnacht S, Beguería S and Latron J (2011) Variability of snow depth at the plot scale: implications for mean depth estimation and sampling strategies.

*The Cryosphere*, **5**(3), 617–629 (doi: 10.5194/tc-5-617-2011)

MacDougall AH and Flowers GE (2011) Spatial and temporal transferability of a distributed energy-balance glacier melt model. *Journal of Climate*, **24**(5), 1480–1498 (doi: 10.1175/2010JCLI3821.1)

Machguth H, Eisen O, Paul F and Hoelzle M (2006) Strong spatial variability of snow accumulation observed with helicopter-borne GPR on two adjacent Alpine glaciers. *Geophysical Research Letters*, **33**(13) (doi: 10.1029/2006GL026576)

Madigan D and Raftery AE (1994) Model Selection and Accounting for Model Uncertainty in Graphical Models Using Occam's Window. *Journal of the American Statistical Association*, **89**(428), 1535–1546, ISSN 01621459

Marshall HP, Koh G, Sturm M, Johnson J, Demuth M, Landry C, Deems J and Gleason J (2006) Spatial variability of the snowpack: Experiences with measurements at a wide range of length scales with several different high precision instruments. In *Proceedings ISSW*, 359–364

McGrath D, Sass L, O'Neel S, Arendt A, Wolken G, Gusmeroli A, Kienholz C and McNeil C (2015) End-of-winter snow depth variability on glaciers in Alaska. *Journal of Geophysical Research: Earth Surface*, **120**(8), 1530–1550 (doi: 10.1002/2015JF003539)

Metropolis N and Ulam S (1949) The Monte Carlo Method. *Journal of the American Statistical Association*, **44**(247), 335–341, ISSN 01621459

Molotch N, Colee M, Bales R and Dozier J (2005) Estimating the spatial distribution of snow water equivalent in an alpine basin using binary regression tree models: the impact of digital elevation data and independent variable selection. *Hydrological Processes*, **19**(7), 1459–1479 (doi: 10.1002/hyp.5586)

Mott R, Faure F, Lehning M, Löwe H, Hynek B, Michlmayer G, Prokop A and Schöner W (2008) Simulation of seasonal snow-cover distribution for glacierized sites on Sonnblick, Austria, with the Alpine3D model. *Annals of Glaciology*, **49**(1), 155–160 (doi: 10.3189/172756408787814924)

Musselman KN, Pomeroy JW, Essery RL and Leroux N (2015) Impact of windflow calculations on simulations of alpine snow accumulation, redistribution and ablation. *Hydrological Processes*, **29**(18), 3983–3999 (doi: 10.1002/hyp.10595)

Raftery AE, Madigan D and Hoeting JA (1997) Bayesian Model Averaging for Linear Regression Models. *Journal of the American Statistical Association*, **92**(437), 179–191 (doi: 10.1080/01621459.1997.10473615)

Réveillet M, Vincent C, Six D and Rabatel A (2016) Which empirical model is best suited to simulate glacier mass balances? *Journal of Glaciology*, 1–16 (doi: 10.1017/jog.2016.110)

Roustant O, Ginsbourger D and Deville Y (2012) DiceKriging, DiceOptim: Two R packages for the analysis of computer experiments by kriging-based metamodeling and optimization. *Journal of Statistical Software*, **21**, 1–55

Schneiderbauer S and Prokop A (2011) The atmospheric snow-transport model: SnowDrift3D.

*Journal of Glaciology*, **57**(203), 526–542 (doi: 10.3189/002214311796905677)

Schuler TV, Crochet P, Hock R, Jackson M, Barstad I and Jóhannesson T (2008) Distribution of snow accumulation on the Svartisen ice cap, Norway, assessed by a model of orographic precipitation. *Hydrological Processes*, **22**(19), 3998–4008, ISSN 1099-1085 (doi: 10.1002/hyp.7073)

Shea C and Jamieson B (2010) Star: an efficient snow point-sampling method. *Annals of Glaciology*, **51**(54), 64–72 (doi: 10.3189/172756410791386463)

Sold L, Huss M, Hoelzle M, Andereggen H, Joerg PC and Zemp M (2013) Methodological approaches to infer end-of-winter snow distribution on alpine glaciers. *Journal of Glaciology*, **59**(218), 1047–1059 (doi: 10.3189/2013JoG13J015)

Tangborn WV, Krimmel RM and Meier MF (1975) A comparison of glacier mass balance by glaciological, hydrological and mapping methods, South Cascade Glacier, Washington. *International Association of Hydrological Sciences Publication*, **104**, 185–196

Taylor-Barge B (1969) The summer climate of the St. Elias Mountain region. Technical report, DTIC Document

Thibert E, Blanc R, Vincent C and Eckert N (2008) Instruments and Methods Glaciological and volumetric mass-balance measurements: error analysis over 51 years for Glacier de Sarennes, French Alps. *Journal of Glaciology*, **54**(186), 522–532

Trujillo E and Lehning M (2015) Theoretical analysis of errors when estimating snow distribution through point measurements. *The Cryosphere*, **9**(3), 1249–1264 (doi: 10.5194/tc-9-1249-2015)

Turcan J and Loijens H (1975) Accuracy of snow survey data and errors in snow sampler measurements. In *32nd Eastern Snow Conference*, 2–11

Walmsley APU (2015) Long-term observations of snow spatial distributions at Hellstugubreen and Gråsubreen, Norway

Wetlaufer K, Hendrikx J and Marshall L (2016) Spatial Heterogeneity of Snow Density and Its Influence on Snow Water Equivalence Estimates in a Large Mountainous Basin. *Hydrology*, **3**(1), 3 (doi: 10.3390/hydrology3010003)

Winstral A, Marks D and Gurney R (2013) Simulating wind-affected snow accumulations at catchment to basin scales. *Advances in Water Resources*, **55**, 64–79, ISSN 0309-1708 (doi: 10.1016/j.advwatres.2012.08.011), snow–Atmosphere Interactions and Hydrological Consequences

Winther J, Bruland O, Sand K, Killingtveit A and Marechal D (1998) Snow accumulation distribution on Spitsbergen, Svalbard, in 1997. *Polar Research*, **17**, 155–164

Woo MK and Marsh P (1978) Analysis of Error in the Determination of Snow Storage for Small High Arctic Basins. *Journal of Applied Meteorology*, **17**(10), 1537–1541 (doi: 10.1175/1520-0450(1978)017¡1537:AOEITD¿2.0.CO;2)

Wood WA (1948) Project "Snow Cornice": the establishment of the Seward Glacial research station. *Arctic*, 107–112

Work R, Stockwell H, Freeman T and Beaumont R (1965) Accuracy of field snow surveys. Technical report

Zhang W and Montgomery DR (1994) Digital elevation model grid size, landscape representation, and hydrologic simulations. *Water Resources Research*, **30**(4), 1019–1028, ISSN 1944-7973 (doi: 10.1029/93WR03553)

## SUPPLEMENTARY MATERIAL

*Topographic parameters*

Topographic parameters are easy-to-calculate proxies for physical processes, such as orographic precipitation, solar radiation effects, wind redistribution and preferential deposition. We derive all parameters (Table **??**) for our study from a SPOT-5 DEM ($40 \times 40$ m) (Korona and others, 2009). Two DEMs are stitched together to cover the Donjek Range. An iterative 3D-coregistration algorithm (Berthier and others, 2007) is used to correct the horizontal ($\sim$2 m E, $\sim$4 m N) and vertical (5.4 m) discrepancy between the two DEMs before stitching.

Visual inspection of the curvature fields calculated using the full DEM shows a noisy spatial distribution. To find an appropriate scale at which the relevant curvature is calculated, various smoothing algorithms and sizes are applied and the combination that produces the highest correlation between curvature and gridcell-averaged WB is chosen. Inverse-distance weighted, Gaussian and gridcell-average smoothing methods, all with window sizes of $3 \times 3$, $5 \times 5$, $7 \times 7$ and $9 \times 9$ gridcells are used. Gridcell-average smoothing with a $7 \times 7$ window resulted in the highest overall correlation between curvature (second derivative) and gridcell-averaged WB as well as slope (first derivative) and gridcell-averaged WB. We use the smoothed DEM to calculate curvature ($\kappa$), slope ($m$), aspect ($\alpha$) and "northness" ($N$).
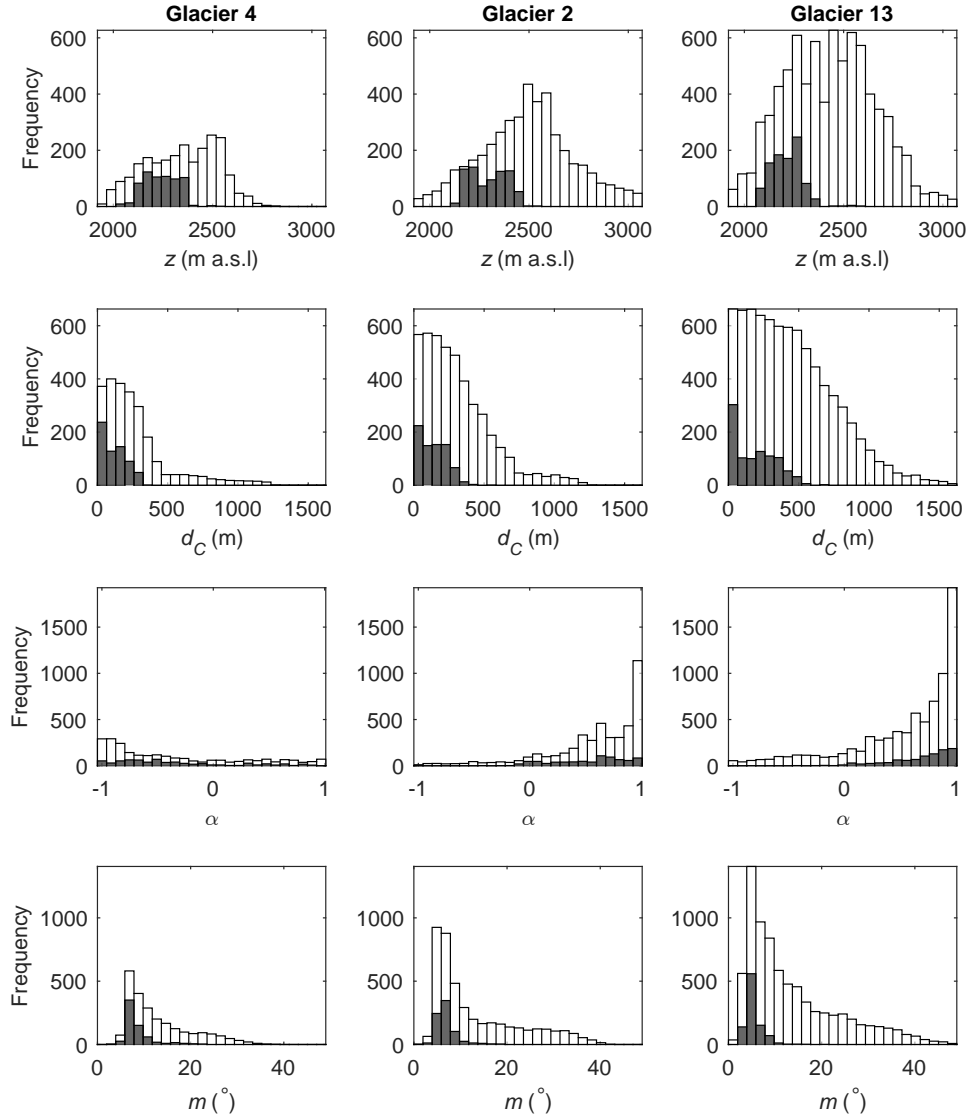
**Fig. 10.** Distribution of sampled (gray bars) and all (white bars) topographic parameters for over Glacier 4 (left column), Glacier 2 (middle column) and Glacier 13 (right column). From top to bottom, topographic parameters are elevation ($z$), distance from centreline ($d_C$), aspect ($\alpha$), slope ($m$), northness ($N$), mean curvature ($\kappa$), and wind redistribution ($Sx$).
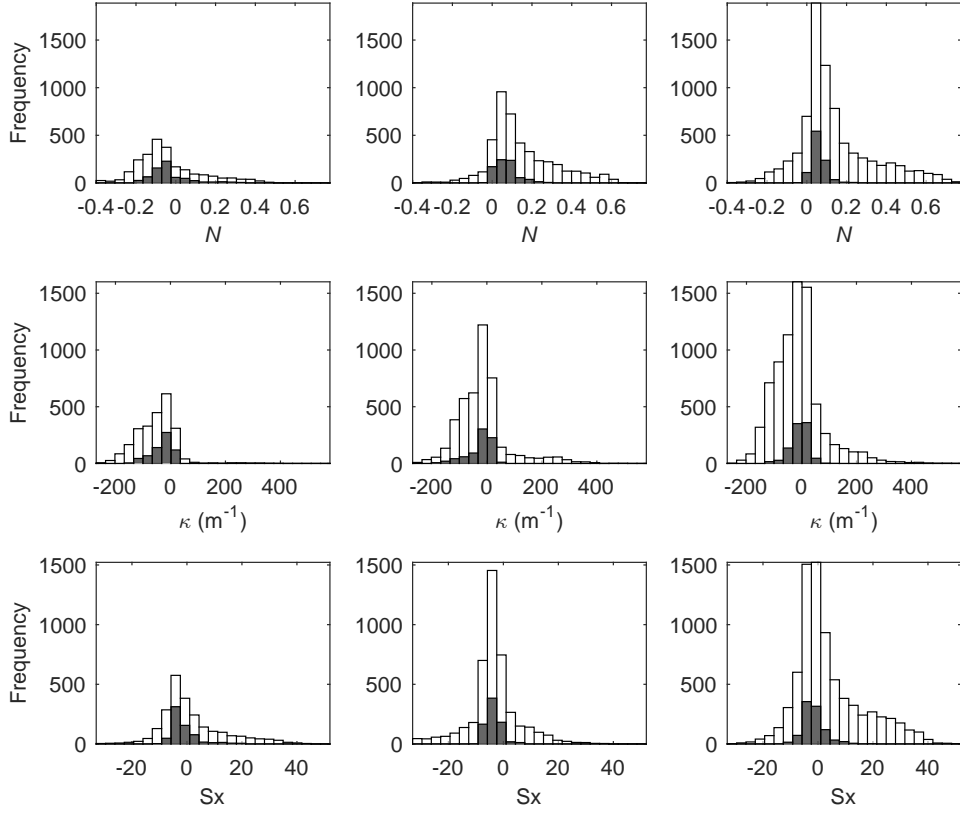
**Fig. 11.** See Fig. 10

**Table 5.** Snow density values used for interpolating density based on snow pit (SP) densities and Federal Sampler (FS) densities. Four interpolation methods are chosen: (1) using a mean snow density for all three glaciers (Range mean density), (2) using a mean density for each glacier (Glacier mean density), (3) using a regression between density and elevation (Elevation regression), and (4) inverse-distance weighted mean density (not shown).

| | | SP-derived density (kg m$^{-3}$) | | FS-derived density (kg m$^{-3}$) | |
|---|---|---|---|---|---|
| | | *Mean* | *STD or $R^2$* | *Mean* | *STD or $R^2$* |
| **S1 or F1** | | 342 | 26 | 318 | 42 |
| | G4 | 348 | 13 | 355 | 18 |
| **S2 or F2** | G2 | 333 | 26 | 286 | 34 |
| | G13 | 349 | 38 | 316 | 41 |
| | G4 | $0.03z + 274$ | 0.16 | $-0.16z + 714$ | 0.53 |
| **S3 or F3** | G2 | $-0.14z + 659$ | 0.75 | $0.24z - 282$ | 0.72 |
| | G13 | $-0.20z + 802$ | >0.99 | $0.12z + 33$ | 0.21 |

**Table 6.** Range and nugget values for simple kriging interpolation

| | Range (m) | Nugget ($\times 10^3$ m w.e.) |
|---|---|---|
| **G4** | 90 | 10.5 |
| **G2** | 404 | 3.6 |
| **G13** | 444 | 4.8 |